# Phonons in isotopically disordered Ge

P. Etchegoin, H. D. Fuchs, J. Weber, and M. Cardona
*Max-Planck-Institut für Festkörperforschung, Heisenbergstrasse 1, D-70569 Stuttgart, Germany*

L. Pintschovius and N. Pyka
*Kernforschungszentrum Karlsruhe, Institut für Nukleare Festkörperphysik, Postfach 3640, D-7500, Karlsruhe, Germany*

K. Itoh and E. E. Haller
*University of California, Berkeley and Lawrence Berkeley Laboratory, Berkeley, California 94720*
(Received 6 April 1993; revised manuscript received 6 July 1993)

We report Raman- and neutron-scattering, infrared-transmission, and photoluminescence experiments in a series of isotopically enriched samples of Ge, including natural Ge and an *alloy* $^{70}Ge_{0.5}{}^{76}Ge_{0.5}$. Emphasis is put on the study of disorder-induced effects on the phonon spectra. Results are compared to exhaustive theoretical calculations using the coherent-potential and self-consistent Born approximations. Reasonably good agreement is found between theory and experiment for the former. Data for the dependence of the energy of the $E_1$ interband electronic gap on isotopic mass are also presented.

## I. INTRODUCTION AND OVERVIEW

An intense study of the optical properties of isotopically enriched Ge samples was triggered recently[1] by the ability to separate and alloy the different isotopes of Ge, producing either isotopically pure or intentionally disordered high purity single crystals. The five different stable isotopes of germanium allow innumerable possibilities to grow pure or disordered crystals in terms of the isotopic content. The study of the disorder-induced features in the phonon or electron states of the crystal via isotopes addresses questions such as the applicability of the coherent-potential approximation (CPA), as a mean-field theory, for weak forms of disorder. Unlike topological or structural disorder (such as in amorphous solids or in liquids), isotopic disorder falls within the classification of substitutional disorder (sometimes called "cellular or chemical disorder," i.e., the same as in binary alloys, mixed crystals,[2] etc.), but with the advantage of being the simplest form of disorder within this category. The comparison of experimental findings to theoretical predictions in the case of disordered systems is most of the time hampered by the approximations involved in the theory. Simple forms of disorder are useful in that sense; they yield a unique opportunity of testing the validity and applicability of different theoretical approaches. Germanium crystals are ideally suited for that purpose and might be taken as a criterion to analyze similar cases.

In this paper we investigate the phonon spectra of two different isotopically disordered samples, i.e., natural Ge and the *alloy* $^{70}Ge_{0.5}{}^{76}Ge_{0.5}$ using as a reference the spectra of isotopically enriched samples of $^{70}Ge$, $^{74}Ge$, and $^{76}Ge$ that have already been discussed in the literature. Our experimental survey includes optical measurements [Raman scattering, infrared (IR) transmittance, and photoluminescence (PL)] as well as measurements of the TO and LO optical phonon branches using inelastic neutron scattering. The experiments are analyzed in the light of CPA calculations[3,4] and the self-consistent Born approximation (SCBA).

An historical account of the study of the isotope effect in Ge must start with the pioneering work of Geballe and Hull,[5] who demonstrated the importance of isotopic scattering in controlling the thermal conductivity above 2 K, and might end with the recent work on disorder-induced features in the Raman spectra of Ge.[24] General as well as specific references to this problem from both experimental and theoretical points of view are given in Refs. 1, 2, and 5–32.

The structure of the present paper is as follows: Section II provides a brief description of the experimental techniques and sample characteristics. An outline of the procedure followed in the CPA and SCBA calculations is given in Sec. III. Section IV presents the experimental results, data evaluation, and comparison between theory and experiment. Finally, Sec. V presents the conclusions.

## II. EXPERIMENT

### A. Samples

All samples, except for the $^{70}Ge_{0.5}{}^{76}Ge_{0.5}$, have been described elsewhere.[13,14,20,21,23,24] The details of the growth technique have been reported in Ref. 32. The sample ($^{70}Ge_{0.5}{}^{76}Ge_{0.5}$) has been grown intentionally to maximize the effects of isotopic disorder. The exact isotopic composition of this sample, as determined by

 

secondary-ion-mass spectroscopy (SIMS), is $^{70}$Ge (50%), $^{72}$Ge (2.1%), $^{73}$Ge (0%), $^{74}$Ge (6.7%), and $^{76}$Ge (41.2%). The sample had a rather high Cu contamination[25] ($\sim 2 \times 10^{14}$ cm$^{-1}$) of no relevance in the evaluation of our experiments. The donor and acceptor concentrations are estimated to be well below $\sim 10^{14}$ cm$^{-3}$.

The dimensionless isotopic-disorder parameter ($g$) (Refs. 13, 14, 20, and 23, 24) is defined as

$$g = \sum_i x_i \left[1 - \frac{m_i}{\overline{m}}\right]^2, \quad (1)$$

where $x_i$ is the concentration of the isotope $i$ with mass $m_i$ ($\sum_i x_i = 1$), and $\overline{m}$ is the average mass. For natural Ge $g_{\rm nat} = 5.874 \times 10^{-4}$, while for the $^{70}$Ge$_{0.5}$ $^{76}$Ge$_{0.5}$ sample $g_{70/76} = 1.556 \times 10^{-3}$. The latter is roughly 50 times the $g$ parameter of one of the isotopically enriched samples (for example in $^{70}$Ge, $g_{70} = 2.976 \times 10^{-5}$).

For the optical experiments the crystals were mechanically polished and etched following standard procedures.[33,34]

### B. Experimental techniques

The high-resolution and multichanel Raman experiments as well as the Fourier transform far-IR transmittance and the edge photoluminescence were performed under the same experimental conditions of Refs. 13, 14, 20, 21, 23, and 24. Inelastic neutron-scattering was measured with a triple axis spectrometer at the ORPHEE reactor in Saclay. Cu[111] and pyrolithic graphite [002] were used as monochromator and analyzer, respectively. The measurements were performed on a natural and an enriched $^{76}$Ge crystal of identical shape ($\sim$20×20×3 mm$^3$). The $^{70}$Ge$_{0.5}$ $^{76}$Ge$_{0.5}$ sample was too small to be studied with sufficient accuracy within available time. The LO[100], TO[100], and TO[111] branches were investigated from the Brillouin zone center to the zone boundary. Several series of scans were performed with alternately the natural Ge sample and the isotopically enriched one to check reproducibility.

## III. THEORY

### A. Self-consistent Born approximation (SCBA)

The SCBA is based on second-order self-consistent perturbation theory, where the self-consistency is expected to include ladder diagrams beyond second order. The complex self-energy $\Sigma(\omega)$ of phonons with frequency $\omega$ reads

$$\Sigma(\omega) = \frac{\omega^2 g}{24N} \int_0^{\Omega_{\rm max}} \frac{2\Omega\rho(\Omega)d\Omega}{[\Omega^2 - \omega^2 - 2\omega\Sigma(\omega)]}, \quad (2)$$

where $g$ is given by (1), $N$ is the number of units cells in the crystal, $\rho(\omega)$ the one-phonon density of states, and $\Omega_{\rm max}$ the cutoff frequency. Approximate expressions for real and imaginary parts of the self-energy of the zone-center optical phonons have been given in Ref. 14. Equation (2) is solved numerically by iterating a first guess for $\Sigma(\omega)$ (usually the non-self-consistent Born approximation). The convergence is fast (typically 50 iterations, depending on $g$) but the final result is very sensitive to the details of the one-phonon density of states (DOS) being used for the numerical evaluation of the integral. In Ref. 13 calculations were performed using the theoretical DOS of $^{70}$Ge from the bond-charge model (BCM). The resulting density of states for $^{70}$Ge, and that obtained for natural Ge using the CPA (see next subsection), together with the experimental determination from neutron scattering[17] are plotted in Fig. 1. The different DOS's are normalized so that the total number of states is the same (6 per unit cell). Note the differences in the region of the optical branches ($\sim$ 250–320 cm$^{-1}$). In particular, Weber's BCM (Refs. 15 and 16) is ill suited for obtaining the $\rho(\omega) \sim \sqrt{(\Omega_{\rm max} - \omega)}$ behavior near the zone-center optical phonons. To avoid this problem, we used the experimental DOS (Ref. 17) (from neutron scattering; see Fig. 1) in Eq. (2). The real and imaginary parts of the self-consistent $\Sigma(\omega)$ calculated with the SCBA [Eq. (2)] are shown in Figs. 2(a–d) and compared with the experimental disorder-induced self-energies in the next section.

### B. Coherent-potential approximation (CPA)

The CPA treats incorrectly multiple scattering associated with clusters.[3]. In mixed alloys the appearance of such states requires further improvements such as the cluster expansion.[2] Computational complications from the point of view of Raman scattering arise from the microscopic models for the electric susceptibility. The case of isotopic substitution in Ge is particularly simple in several ways. First, it simplifies the problem of the

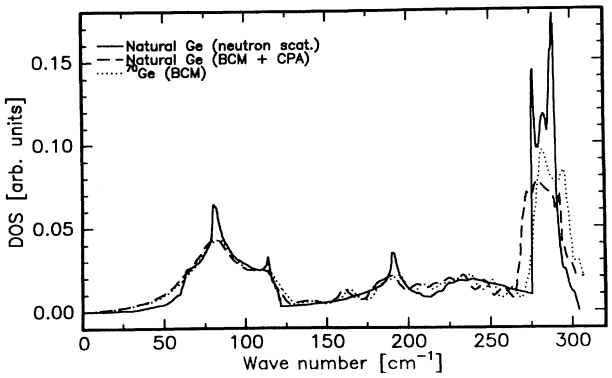


FIG. 1. Vibrational DOS of Ge. The experimental results were obtained from inelastic neutron-scattering data in natural Ge (Ref. 17). The curve labeled $^{70}$Ge represents the DOS from the BCM calculated in Ref. 13 as well as the corresponding result for natural Ge provided the multiple-scattering corrections predicted by the CPA are added (Ref. 13). The frequencies in the case of $^{70}$Ge have been scaled ($\sim 1/\sqrt{m}$) to take into account the difference in mass with respect to the average $\overline{m}$ of natural Ge. Instead of using the BCM output for the calculations we employed the result of Nilsson and Nelin (Ref. 17) (neutron scattering) to calculate $\Sigma(\omega)$ in both Eqs. (2) and (3).

polarizability since the replacement is being done with the same atomic species; i.e., the electronic structure is, to first order, unperturbed. Thus, the isotopically disordered lattice constitutes a medium in which, to a very good approximation, the electrons are unperturbed and the phonons experience "diagonal-disorder."[30] This suggests the applicability of the simplest ansatz for the polarizability: a bond-polarizability model. Further simplification comes from the absence of localization effects. Roughly speaking, localization is an interplay between the strength of the potential and the bandwidth and, in this case, cannot take place; thus CPA is expected to work reasonably well. At the same time, it is possible to show that CPA constitutes the best single-site approximation that takes into account all essentially single-site diagrams.[4]

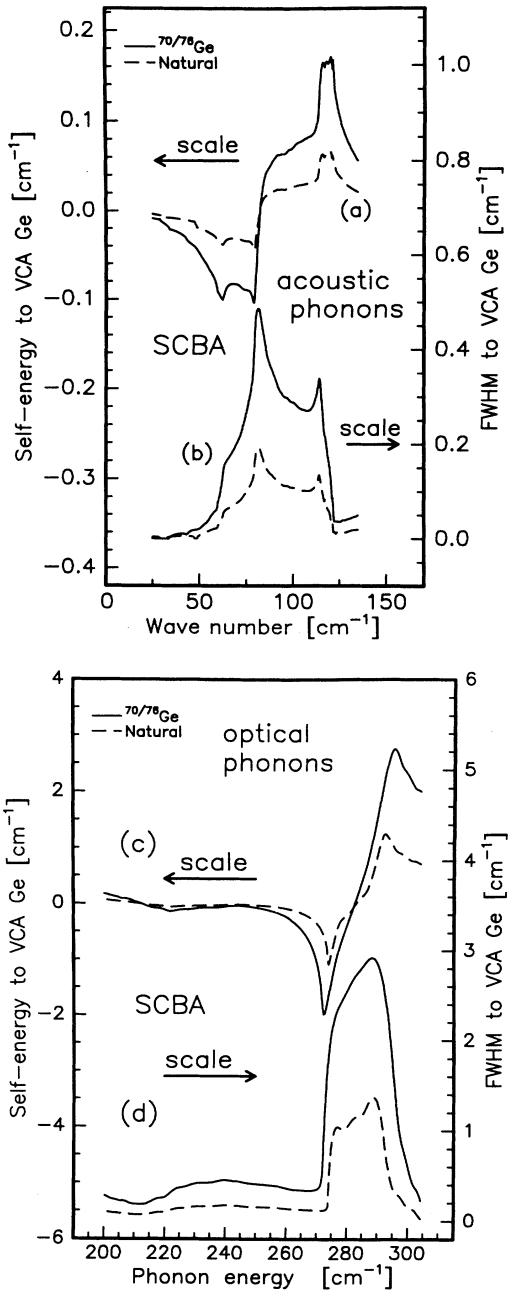


FIG. 2. SCBA results, (a) and (b) are the real and imaginary parts of $\Sigma(\omega)$ (self-energy and FWHM, respectively) in the region of the acoustic phonons (see Fig. 1), for natural Ge and $^{70}Ge_{0.5}\,^{76}Ge_{0.5}$. In (c) and (d), $\Sigma(\omega)$ is shown in the optical phonon region. Note that $\mathrm{Re}\,[\Sigma(\omega)]$ scales like $g$ for the phonons at $\Gamma$ ($\sim$ 310 cm$^{-1}$), which are observable with Raman spectroscopy. The latter does not hold in regions where $\mathrm{Im}\,[\Sigma(\omega)] \neq 0$. All values are given with respect to a zero defined by the virtual crystal approximation (VCA) of average mass $\overline{m}$.

In Fig. 3 we show the real and imaginary parts of $\Sigma(\omega)$ for natural Ge and $^{70}Ge_{0.5}\,^{76}Ge_{0.5}$. In the region of the acoustic and optical phonons. The calculation has been performed by solving the fifth-order complex equation for the zero average scattering,[4]

$$\sum_{i=1}^{5} \frac{x_i \left\{M_{\mathrm{VC}}\omega^2\left[1-\tilde{\varepsilon}(\omega)\right]-m_i\omega^2\right\}}{1-\left\{M_{\mathrm{VC}}\omega^2\left[1-\tilde{\varepsilon}(\omega)\right]-m_i\omega^2\right\}G(\omega^2,\tilde{\varepsilon}(\omega))} = 0, \tag{3}$$

where $M_{\mathrm{VC}} = \sum_{i=1}^{5} x_i m_i$ is the mass of the virtual crystal formed by the five different isotopes $x_i$, $\tilde{\varepsilon}(\omega)$ the "dimensionless self-energy," and $G(\omega^2,\tilde{\varepsilon}(\omega))$ the one-particle Green function given by

$$G(\omega^2,\tilde{\varepsilon}(\omega)) = \frac{1}{NM_{\mathrm{VC}}}\int_0^{\Omega_{\max}} \frac{\rho(\Omega)d\Omega}{\omega^2\left[1-\tilde{\varepsilon}(\omega)\right]-\Omega^2}. \tag{4}$$

Equations (3) and (4) are solved self-consistently using the DOS from neutron scattering in (4) and a first guess for $\tilde{\varepsilon}(\omega)$. The only physical root of (3) is easy to distinguish because the others tend to diverge as the number of iterations is increased. The energy shift ($\mathrm{Re}\,[\Sigma_{\mathrm{CPA}}(\omega)]$) and the disorder-induced full width at half maximum (FWHM) ($\mathrm{Im}\,[\Sigma_{\mathrm{CPA}}(\omega)]$) are related to $\tilde{\varepsilon}(\omega)$ by

$$\mathrm{Re}\,[\Sigma_{\mathrm{CPA}}(\omega)] \sim \hbar\omega \left\{1/\sqrt{\left(1-\mathrm{Re}\,[\tilde{\varepsilon}(\omega)]\right)}-1\right\} \tag{5}$$

and

$$\mathrm{Im}\,[\Sigma_{\mathrm{CPA}}(\omega)] = -\hbar\omega\ \mathrm{Im}\,[\tilde{\varepsilon}(\omega)], \tag{6}$$

where $\hbar\omega$ are phonon frequencies of the virtual crystal.

Note the similarities between Figs. 3(a–b) (CPA) and Figs. 2(a–b) (SCBA) for the acoustic phonon branches except for some differences in the absolute amplitude of the peaks. The region $\sim$ 260–320 cm$^{-1}$, corresponding to the optical branches, is more involved and the SCBA presents substantial qualitative differences when compared with the CPA output. We shall show that CPA is in better agreement with the experiment in the next section. Equivalent results for the CPA self-energy of diamond can be found in Ref. 12. Note the appearance of "oscillations" in both the real and imaginary parts of the $\Sigma_{\mathrm{CPA}}(\omega)$ denoting the appearance of strong resonances in the continuum.[27,28] We used the CPA Green function to calculate not only the self-energies of the phonons but also to compute the disorder-induced first-order Raman

scattering in the region of the acoustic phonons. The latter complements the results for the TO phonons presented in Ref. 24. The comparison with experiments as well as further discussion of both theoretical approaches are given in Sec. IV.

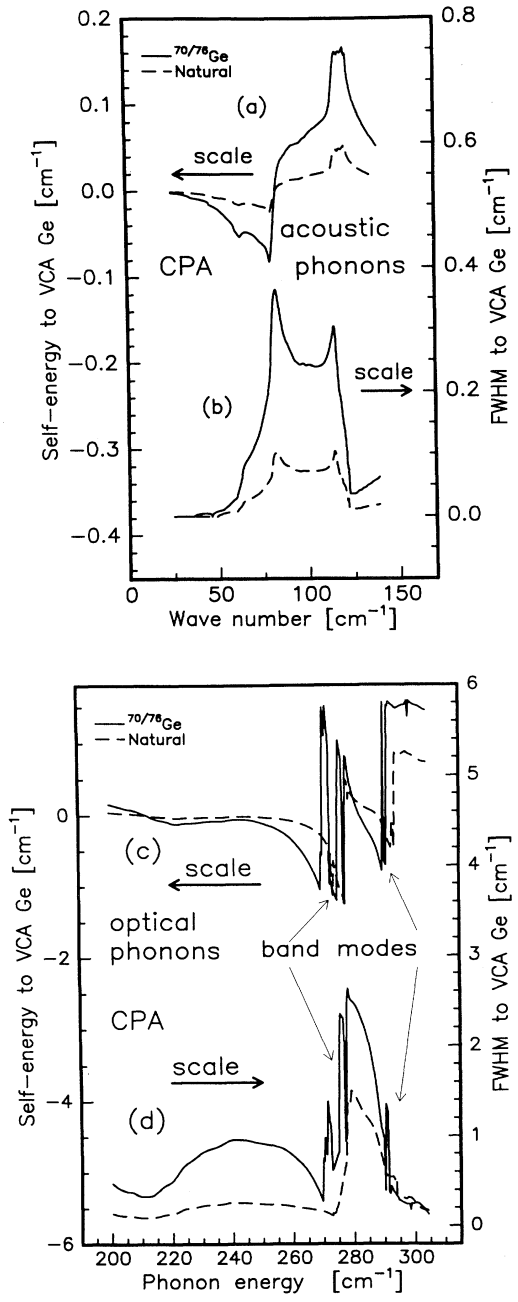


FIG. 3. CPA results in the phonon energy region of Fig. 2. All values are given with respect to the VCA. The optical phonon region shows strong differences with respect to the SCBA of Fig. 2. The appearance of band modes close to the sharp edges of the DOS (see Fig. 1) is appropiatelly labeled. These states are responsible for disorder-induced Raman activity as shown in Ref. 24.

## IV. EXPERIMENTS

### A. Results

(i) Inelastic neutron scattering: In Fig. 4(a) we show the LO optical phonon branch from $\Gamma$ to $X$ obtained for a $^{76}$Ge enriched crystal and a natural one. Measurements of the TO branch are shown in Fig. 4(b). The latter include the mapping of the branches along two different lines in the reciprocal space with a different orientation of the resolution ellipsoid with respect to the dispersion surface (focusing and defocusing conditions). The frequencies of the $^{76}$Ge crystal have been multiplied by 1.0208, thus eliminating the trivial proportionality to $1/\sqrt{m}$. The differences that are left should be solely due to disorder. Although these differences are small, it is possible to discern systematic deviations between the experimental values of the enriched and natural samples. The change in the broadening of the peaks can also be evaluated. Particular attention has been paid to the self-energy and broadening of the TO phonons at $\Gamma = (0,0,0)$, $L = 2\pi/a(0.5,0.5,0.5)$, $W = 2\pi/a(1,0.5,0)$, and $X = 2\pi/a(1,0,0)$. The neutron results are discussed, together with those from other experiments, in the next subsection. The numerical values for the energy shift of the TO phonons at the above mentioned points are summarized in Table I.

(ii) Photoluminescence: The edge PL data at $T = 1.8$ K and 4.2 K for the complete set of isotopically enriched samples and a natural one are displayed in Figs. 5(a–b). The luminescence of the electron-hole liquid[35] (EHL) droplets, mediated by LA, TA, and TO phonon emission, dominates at the lowest temperature in Fig. 5(a). The LA-phonon-assisted recombination of the free exciton is visible at $T = 1.8$ K in Fig. 5(a). The zero-phonon recombination of excitons bound to neutral impurities is also observed ($BE^{NP}$). The $^{70}Ge_{0.5}$ $^{76}Ge_{0.5}$ sample in Fig. 5(a) exhibits an additional peak close to the $BE^{NP}$ due to the presence of copper.[36,37] The latter represents the zero-phonon recombination of an exciton bound to copper (which we know to exist in the $^{70}Ge_{0.5}$ $^{76}Ge_{0.5}$ sample). Note dependence of the peaks on the average mass which can be observed with the naked eye. In Fig. 5(b) the luminescences of a pure sample ($^{76}$Ge), natural Ge , and $^{70}Ge_{0.5}$ $^{76}Ge_{0.5}$ are shown at $T = 4.2$ K. In $^{76}$Ge and natural Ge the TO- and LA-phonon-assisted recombination of the free exciton coexists with rests of the luminescence due to the EHL. This is due to the particular laser power used. In the $^{70}Ge_{0.5}$ $^{76}Ge_{0.5}$, however, under the same experimental conditions, the EHL luminescence vanishes possibly due to the lifetime reduction introduced by the rather high amount of Cu deep levels. Phonon-assisted recombination from the free exciton and from excitons bound to either neutral impurities or Cu can be observed. The PL data can be used for evaluating phonon self-energies as follows: From Figs. 3(a–d) LA and TA phonons are expected to have a negligible disorder-induced self-energy; thus, by evaluating the difference between the phonon-assisted luminescences through LA and TO phonons the shifts of the latter can be obtained. This procedure eliminates automatically

the electronic part of the shifts due to $e$-ph interaction (see Refs. 22 and 23 for details). These experiments can be compared with results in Ref. 25.

(iii) IR transmittance: The infrared transmission of the most disordered sample $^{70}Ge_{0.5}\,^{76}Ge_{0.5}$ at $T = 100$ K is compared to that of the enriched $^{76}Ge$ sample in

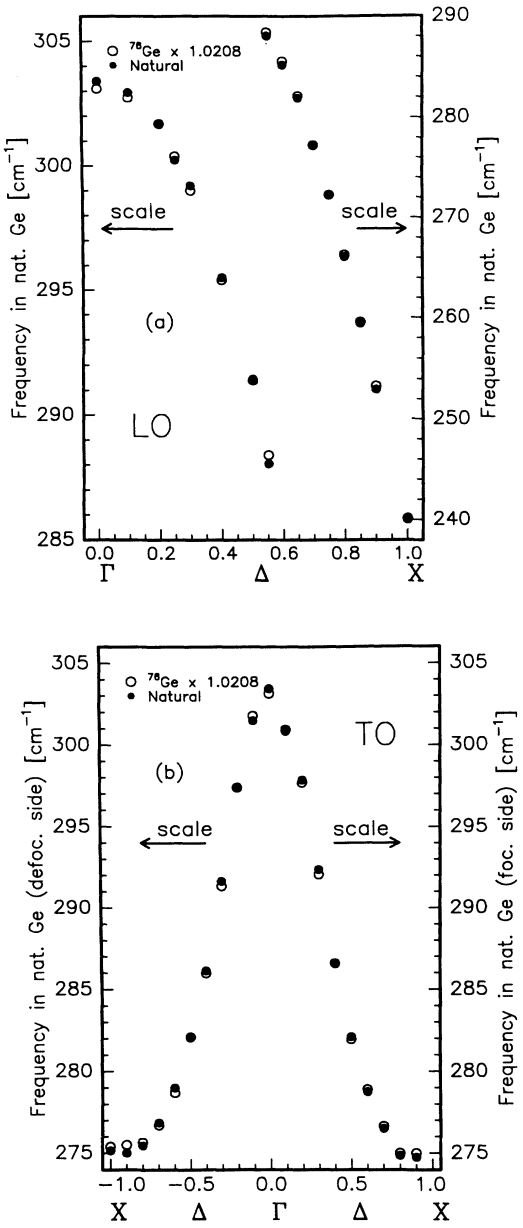


FIG. 4. Inelastic neutron-scattering results. In (a), the LO phonon branch is displayed. The frequencies of the isotopically enriched sample $^{76}Ge$ were multiplied by 1.0208 so as to eliminate the trivial mass dependence of the phonon frequencies. Differences between the two measurements are due to the isotopic disorder. In (b) results for the LO phonon branch are shown. Two sets of measurements are displayed, for an incident focused or defocused neutron beam (see text for details). Results for TO phonons at particular points of the Brillouin zone are summarized in Table I.

TABLE I. Disorder-induced changes in the frequencies of TO phonons in natural Ge at different points of the Brillouin zone obtained from inelastic neutron scattering.

| Phonon | $\omega_{ph}$ (cm$^{-1}$) | Re[$\Sigma$] (cm$^{-1}$) |
|---|---|---|
| $TO_\Gamma$ | 303 | $0.4 \pm 0.2$ |
| $TO_L$ | 290 | $-0.2 \pm 0.07$ |
| $TO_W$ | 278 | $0.1 \pm 0.15$ |
| $TO_X$ | 275 | $-0.2 \pm 0.07$ |

Fig. 6. The labels indicate the assignments to the two-phonon absorption spectra of natural Ge, as given by Nilsson and Nelin,[17] and are a guide to the eye. Qualitative results can be easily obtained from the IR experiments to compare with calculations. However, as in the case of second-order Raman scattering (see below), the quantitative shifts obtained from two-phonon structures are not very trustworthy. Further comments are given in Sec. IV B.

(iv) First- and second-order Raman scattering: The high-resolution ($\sim$0.06 cm$^{-1}$) off-resonance (laser energy=$E_L$=2.41 eV) first-order Raman spectra of the TO phonons at $T = 80$ K are shown in Fig. 7 for three different samples: a pure one ($^{74}Ge$), natural Ge, and the $^{70}Ge_{0.5}\,^{76}Ge_{0.5}$ *alloy*. The phonon frequencies are scaled so that the trivial square root of the mass dependence and the disorder-induced shifts are eliminated. The small changes in frequency due to the isotopic disorder are of the order of $\sim$1 cm$^{-1}$ for optical zone-center phonons [see Figs. 2(c) and 3(c)]. The changes in width (FWHM) are also small. Nevertheless, differences among the three samples can be observed. Both the frequency shifts and broadenings obtained from Lorentzian fits of the Raman peaks are summarized with the rest of the experiments in the next subsection. The second-order Raman spectra at $T = 80$ K (taken in resonance with the $E_1$ gap) in the region corresponding to the overtone DOS of the optical branches is shown in Fig. 8 for natural Ge and $^{70}Ge_{0.5}\,^{76}Ge_{0.5}$. The extraction of a $\Sigma(\omega)$ from the measured structures is difficult in this case since different critical points are not well resolved. However, the changes in broadening on account of disorder are evident in the figure. The rest of the second-order Raman spectra (for the acoustic branches) is shown in the next subsection.

### B. Comparison with theory

The quality of the calculations is judged in terms of (i) the self-energies of the phonons for the two disordered samples (natural Ge and $^{70}Ge_{0.5}\,^{76}Ge_{0.5}$), (ii) the ability to reproduce the second-order Raman spectra, which for the special case of tetrahedraly bonded semiconductors resembles the density of states in units of $2\omega$ (overtone DOS) (Ref. 38) and therefore can be compared to the imaginary part of the CPA Green function and, finally, (iii) the capability of predicting disorder-induced first- and second-order Raman-scattering features as in Ref. 24. The latter can be experimentally observed after long integration times in particular regions of the spectra

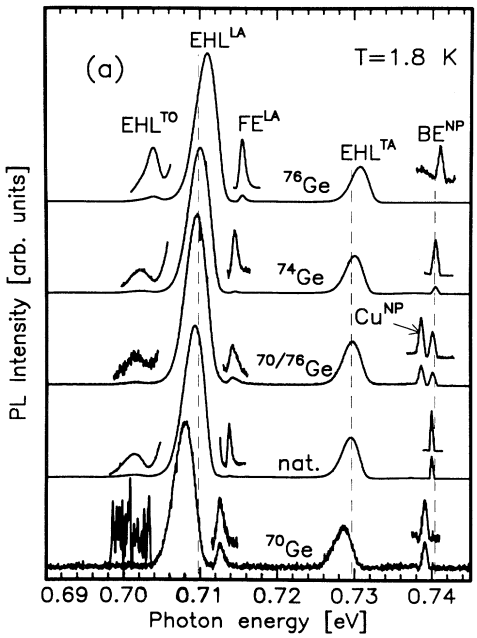


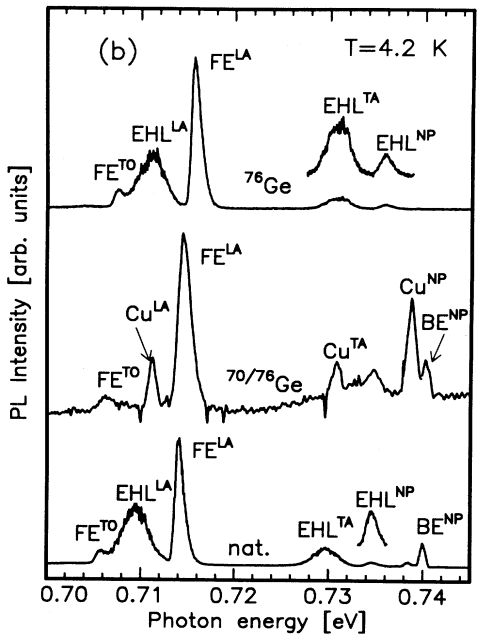


FIG. 5. (a) Edge photoluminescence at $T = 1.8$ K showing the EHL recombination due to TA, LA, and TO phonons, as well as small signs of the phonon-assisted recombination of the free exciton by LA phonons ($FE^{LA}$). The bound exciton recombination with zero-phonon emission can also be observed ($BE^{NP}$). The $^{70}Ge_{0.5}\,^{76}Ge_{0.5}$ sample shows and additional peak close to its $BE^{NP}$ line produced by the presence of copper impurities (Refs. 23 and 25. The weak peaks are multiplied by an arbitrary factor and plotted on top of each curve. (b) PL signal at $T = 4.2$ K. The luminescence of natural Ge and $^{76}Ge$ is dominated by phonon-assisted recombination of free excitons and EHL, while the data for $^{70}Ge_{0.5}\,^{76}Ge_{0.5}$ show signs of recombination by free excitons as well as by excitons bound to Cu impurities (see text for details).

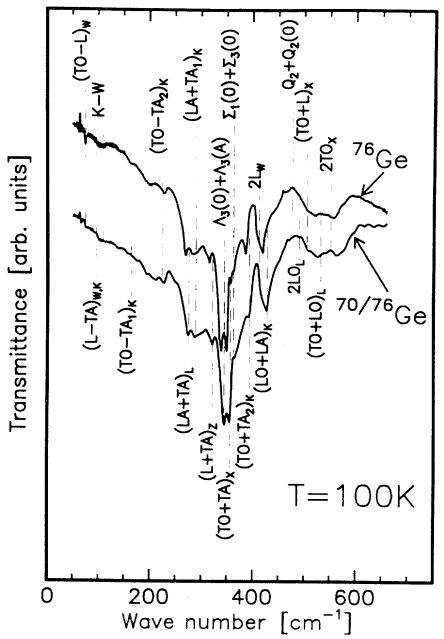


FIG. 6. IR transmittance at $T = 100$ K of the disordered *alloy* $^{70}Ge_{0.5}\,^{76}Ge_{0.5}$ as compared to that of the isotopically enriched $^{76}Ge$ sample under the same conditions. The labels corresponds to the two-phonon emission frequencies in natural Ge according to Ref. 17 and are a guide to the eye.

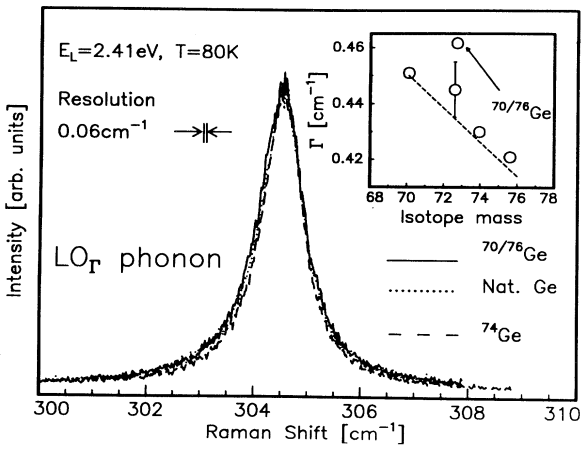


FIG. 7. First order Raman scattering of the TO phonon at $T = 80$ K for $^{70}Ge_{0.5}\,^{76}Ge_{0.5}$, $^{74}Ge$, and natural Ge. The resolution is indicated in the plot. The frequencies are shifted (taking natural Ge as a reference) so that the trivial dependence on $\overline{m}$ and the disorder-induced shift are eliminated. The small changes in the widths can in this way be compared. The inset shows the broadenings of the peaks for the complete set of samples (see Sec. II) as obtained from Lorentzian fits. The dashed line represents the $1/\sqrt{m}$ mass dependence. Deviations from this line are due to isotopic disorder. The experimental frequencies are listed together with the other experimental determinations in Fig. 9.

as explained below.

We analyze first the disorder-induced experimental data for the self-energies of natural Ge which are more extensive than those for $^{70}Ge_{0.5}$ $^{76}Ge_{0.5}$. The results of neutron scattering (Table I), Raman (Fig. 7), and PL [Figs. 5(a–b)], plus the IR and PL data of Refs. 20 and 25 are plotted together with the calculations of Figs. 2(c–d) and 3(c–d) for natural Ge in Fig. 9 in the optical phonon region (see Fig. 1). Several conclusions can be reached. First of all, it is clear from Fig. 9 that the SCBA fails to reproduce the experimental Re[$\Sigma(\omega)$] in the region ~270–310 cm$^{-1}$ where the TO density of states has its substantial contribution (see Fig. 1). The SCBA reproduces roughly the average behavior, but CPA is far superior. The general agreement of the four experimental techniques with CPA is quite good for both real and imaginary parts of the self-energy. However, a problem concerning the frequency shift of the $TO_L$ phonon at ~290 cm$^{-1}$ persists. While neutron scattering predicts a negative shift (see Table I) the optical data give either a positive number (like in our PL experiments or those of Ref. 25) or a negative one (IR transmittance in Ref. 20), much larger than that from neutron scattering (~ 1 cm$^{-1}$). Neutron scattering and PL provide probably the most reliable data, while IR data (based on the two-phonon spectra) are questionable. In any case, PL and neutron scattering give manifestly opposite results for the self-energy of $TO_L$. On the other hand, the proximity of a sharp edge in the real part of the CPA self-energy [Fig. 9(a)] at ~ 290 cm$^{-1}$ makes a definitive

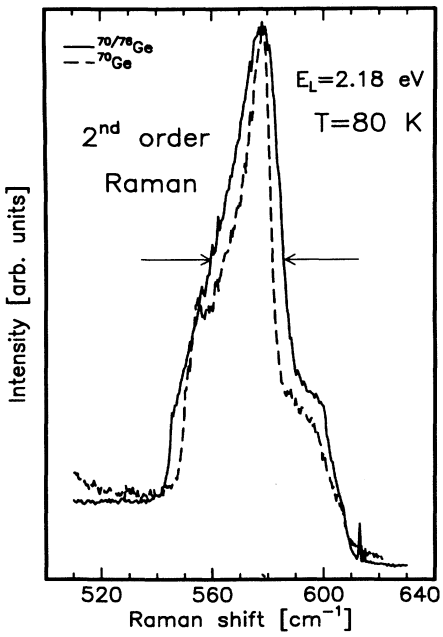


FIG. 8. Second-order Raman spectra in the region of the overtone density of states for optical branches. The data were recorded at $T = 80$ K with the laser in resonance with the $E_1$ gap of Ge. A broadening is seen in going from natural Ge to $^{70}Ge_{0.5}$ $^{76}Ge_{0.5}$ as can be predicted from Figs. 2(d) or 3(d). The frequencies are corrected for the trivial mass dependence as in Fig. 7.

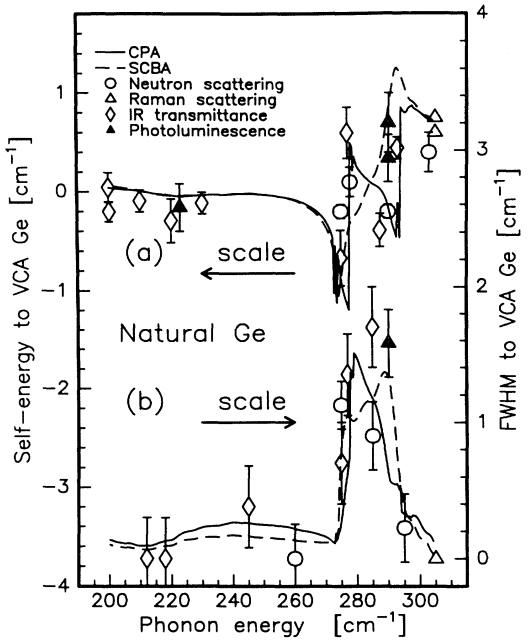


FIG. 9. Disorder-induced complex self-energies of phonons in natural Ge found from neutron- and Raman-scattering, PL, and IR transmittance data. The calculated curves were obtained with the SCBA and CPA methods [Eqs. (2) and (3)], respectively.

answer as to which result is more reliable impossible.[39] We detected that the multiple oscillations of the real part of $\Sigma(\omega)$ are quite sensitive to the the assumed steepness of the DOS in the region of the optical branches. The CPA is in that region rather questionable. Nevertheless, the general quality of the comparison between the 30 experimental points obtained from four different techniques and the parameter-free CPA output is judged to be satisfactory in Fig. 9. The off-resonance second-order Raman scattering for natural Ge is compared with the density of states [overtone DOS in units of $2\omega$ (Ref. 38)] of neutron scattering,[17] a theoretical estimate by means of the BCM,[13] and our CPA output (from the imaginary part of the CPA Green function) in Fig. 10. Our calculation, from which the self-energy of Figs. 3(a–d) and 9 has been obtained, reproduces quite well the experimental overtone DOS of our Raman experiments.[40] Furthermore, we had used a similar CPA calculation to demonstrate the existence of disorder-induced Raman scattering in Ref. 24 in the low-energy tail of the TO zone-center phonon, and we extend here the same argument to the weaker, but observable, features around ~75 cm$^{-1}$. Essentially, if disorder is present, and defining a Raman polarizability proportional to the displacement of the atom $u_i$.[24,30] The average of the squared displacements is done with the formalism of Refs. 27 and 28 but using the CPA Green function. The disorder-activated Raman scattering appears especially in those regions where the one-phonon DOS has sharp edges (see Fig. 1) and may overlap with second-order Raman scattering proportional to the overtone CPA density of states,

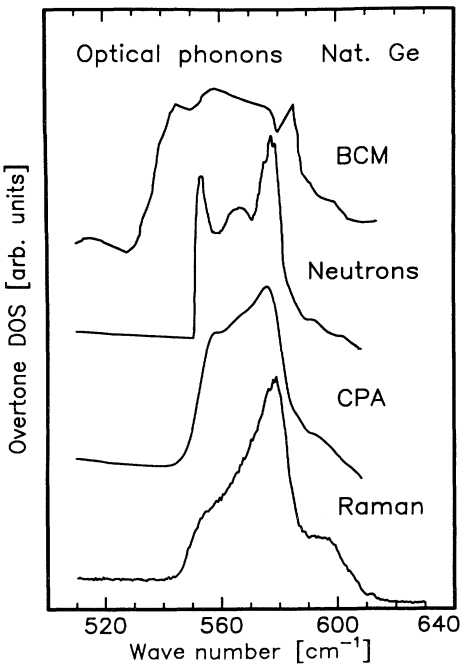


FIG. 10. Comparison of the second-order Raman spectra of natural Ge with the overtone DOS obtained from the BCM (Ref. 13), neutron scattering (Ref. 17), and our CPA results in the optical phonon region. Note that our CPA output reproduces quite well the second-order Raman scattering. Similar results for diamond have been presented in Ref. 12

$$\frac{d^2\sigma}{d\Omega d\omega} \sim \frac{1}{\pi}\mathrm{Im}\left[G((\omega')^2, \tilde{\varepsilon}(\omega'))\right]_{\omega'=2\omega}, \quad (7)$$

in some energy range. In Fig. 11 we display the second-order Raman spectra of $^{70}$Ge, natural Ge, and $^{70}Ge_{0.5}$ $^{76}Ge_{0.5}$ in the region $\sim$ 50–250 cm$^{-1}$ (corresponding to the DOS overtone frequencies of the acoustic branches in Fig. 1). The experiments were performed at T=80 K under resonant excitation [$\hbar\omega_{\mathrm{laser}} = 2.18$ eV], and employing long integration times ($\sim$ 8 h). In the same figure we display the overtone DOS [Eq. (7)] obtained from the CPA for natural Ge and $^{70}Ge_{0.5}$ $^{76}Ge_{0.5}$. In the region $\sim$ 120–250 cm$^{-1}$ both calculations are essentially identical meaning that isotopic disorder has very little effect on the acoustic branches, as mentioned before. The Raman experiments for $^{70}Ge_{0.5}$ $^{76}Ge_{0.5}$ and natural Ge between 120 and 250 cm$^{-1}$ support this conclusion. Below 120 cm$^{-1}$ the one-phonon DOS structure of the acoustic branches (see Fig. 1) gives rise to disorder-induced Raman scattering superimposed on the second-order contribution, producing an additional weak structure centered around $\sim$ 75 cm$^{-1}$. This effect becomes evident if the spectra of the isotopically mixed Ge are compared with that of $^{70}$Ge in the region under discussion. The structure calculated between 50 and 120 cm$^{-1}$ for $^{70}Ge_{0.5}$ $^{76}Ge_{0.5}$ is labeled "disorder induced" in Fig. 11. The predictions of the calculation are reasonably well reproduced by the experiments. Finally, in Table II, the self energies of the critical points of the $^{70}Ge_{0.5}$ $^{76}Ge_{0.5}$ sample are compared with the calculations. Quantitative comparison can be performed with the PL and Raman data while the IR-transmittance results must be reported as only qualitative. In Fig. 6 it is possible to observe that if the two-phonon emission contains one or two optical phonons the structure is broadened or shifted appreciably, as expected from Figs. 3(c–d) [see for example the two-phonon frequencies of $2TO_X$ or $(TO+TA_2)_K$ as compared to that of $(LA+TA)_L$ or

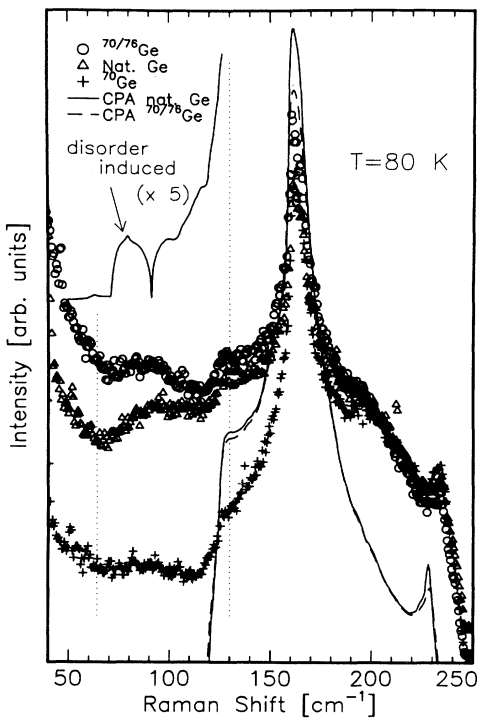


FIG. 11. Second-order Raman scattering in the region of the overtone DOS of TA phonons (all frequencies are normalized to natural Ge as in Figs. 7 and 8). Experimental data are given for $^{70}$Ge, natural Ge, and $^{70}Ge_{0.5}$ $^{76}Ge_{0.5}$. The CPA overtone DOS for $^{70}Ge_{0.5}$ $^{76}Ge_{0.5}$ and natural Ge are also shown. In the region $\sim$ 50–120 cm$^{-1}$ the disorder-induced Raman signal is plotted for $^{70}Ge_{0.5}$ $^{76}Ge_{0.5}$ (with some arbitrary offset). Note the appearance of structure at about $\sim$ 75 cm$^{-1}$ as the disorder is increased, and the presence of increasing "background" in this region.

TABLE II. Self-energies in $^{70}Ge_{0.5}$ $^{76}Ge_{0.5}$ of phonons observable with Raman spectroscopy or PL. The experimental values include the PL data of Ref. 25 and are compared with CPA calculations.

| Phonon | Experiment (cm$^{-1}$) | CPA (cm$^{-1}$) |
|---|---|---|
| $TO_L$ | $1.12 \pm 0.24$[a] | 1.4 |
| | $1.2 \pm 0.3$[b] | |
| $LA_L$ | $-0.4 \pm 0.2$[a] | $-0.1$ |
| $TA_L$ | $0 \pm 0.2$[a] | $-0.04$ |
| $TO_\Gamma$ | 0.98[c] | 1.48 |

[a]PL of Cu impurities from Ref. 25.
[b]PL, present work.
[c]Raman scattering, present work.

$(L+TA)_Z$]. The general qualitative result is in agreement with the theoretical estimate but the numerical values of broadenings and shifts can be extracted with an accuracy not better than $\pm$ 1.5 $cm^{-1}$ (which is of the order of the expected effects). The problem is particularly acute for $^{70}Ge_{0.5}$ $^{76}Ge_{0.5}$ in the region $\sim$ 450–600 $cm^{-1}$ (emission of two optical phonons), as might be anticipated from Figs. 3(c–d). We do not feel confident in assigning a number to the corresponding self-energies.

## V. DISCUSSION AND CONCLUSIONS

Notwithstanding some experimental problems, the overall agreement between the disorder-induced self-energies of the phonons obtained from four different experimental techniques and the CPA calculations make us feel confident that the effects of isotopic disorder on the vibrational properties of Ge are basically understood. The details of the first- and second-order Raman spectra can be predicted quite accurately giving further support to the theory. We thus summarize the facts that either deserve more work or are not understood so far. The real part of $\Sigma(\omega)$ for the $TO_L$ phonons is still controversial and the Raman background observed in the TA region of the isotopically disordered samples does not follow the calculations (see Fig. 11). We were unable to decide whether that background is as a non-**k**-conserving scattering or an experimental artifact. Neutron scattering measurements on a $^{70}Ge_{0.5}$ $^{76}Ge_{0.5}$ sample would help to understand the former question.

Two more interesting facts were not discussed so far. First, the disorder induced Raman scattering reported in Ref. 24, in the $^{70}Ge_{0.5}$ $^{76}Ge_{0.5}$ and natural samples, at the low-energy edge of the TO phonon at $\Gamma$, presents interesting selection rules. In Fig. 12 we summarize the experimental results that complement those given in Ref. 24. In Fig. 12(a), the bottom part of the $LO_\Gamma$ Raman peak is plotted for three samples: $^{70}Ge$, natural Ge, and $^{70}Ge_{0.5}$ $^{76}Ge_{0.5}$. The additional features at the low-energy side of the peak come from disorder-induced first-order Raman scattering.[24] In Figs. 12(b–c) we show the polarization dependence of this structure for a $\langle 100 \rangle$ surface of $^{70}Ge_{0.5}$ $^{76}Ge_{0.5}$. To observe only the disorder-induced part we subtracted a Lorentzian fit to the main $LO_\Gamma$ peak, as in Ref. 24. In Fig. 12(b), (||) refers to a measurement performed with incident polarization $\hat{e}_L \parallel [011]$ and scattered $\hat{e}_S \parallel [011]$, while (|−) means $\hat{e}_L \parallel [011]$ but $\hat{e}_S \parallel [0\bar{1}1]$. In Fig. 12(c) the correspondence is (||): $\hat{e}_L \parallel [010]$, $\hat{e}_S \parallel [010]$; and (|−): $\hat{e}_L \parallel [010]$, $\hat{e}_S \parallel [001]$, respectively. From Ref. 38 it follows that the Raman intensities for these cases are $I^{[011]}_{[011]} \sim |a|^2 + |b|^2 + |d|^2$, $I^{[0\bar{1}1]}_{[011]} \sim 3|b|^2$, $I^{[010]}_{[010]} \sim |a|^2 + 4|b|^2$, and $I^{[001]}_{[010]} \sim |d|^2$, where sub- and superindexes indicate the direction of $\hat{e}_L$ and $\hat{e}_S$, respectively, and $a, b, d$ are three complex numbers denoting the only nonzero components of the symmetric Raman tensors for the $\Gamma_1, \Gamma_{12}$, and $\Gamma_{25'}$ irreducible representations of the $O_h$ point group, respectively. These results imply that the $\Gamma_{15}$ component of the tensor yields the most important contribution to the (||) scattering in Fig. 12(b) and to (|−) in Fig. 12(c). The two other possibilities (|−) and (||) of Figs. 12(b) and (c), respectively, suggest that they are produced mainly by the $\Gamma_{12}$ component and present roughly the correct intensity ratio $\sim 4/3$, i.e., thus is negligible the $\Gamma_1$ component. In order to obtain Raman tensors transforming like $\Gamma_{12}$ one must have inequivalent tetrahedral directions, produced by the random isotope distribution. Note that the $\Gamma_1$ component is also negligible in highly disordered systems such as amorphous $GeO_2$.[49] It is easy to show that the $\Gamma_1$ component should be zero for phonons along [001], [111], and [110] directions. It should therefore remain very small for intermediate low symmetry directions. This makes contact with the second interesting fact that we want to point out. That is the relation, at least from a formal point of view, between isotopic disorder and a "site-percolation" problem. A lattice with isotopic disorder can be thought of as a typical problem of site percolation,[47,48] and has some interesting consequences.

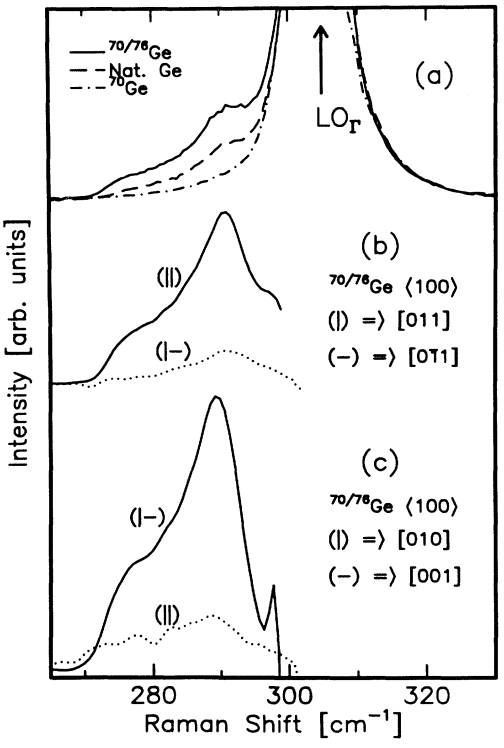


FIG. 12. Selection rules for the disorder-induced first-order Raman scattering at the low-energy edge of the Raman phonon peak (Ref. 24). In (a) we show the raw data. The peaks are scaled to the frequency of natural Ge in order to correct the trivial mass dependence. The bottom part of the $LO_\Gamma$ Raman phonon peak is shown for three samples: $^{70}Ge_{0.5}$ $^{76}Ge_{0.5}$, nat. Ge, and $^{70}Ge$. The additional features in the natural and $^{70}Ge_{0.5}$ $^{76}Ge_{0.5}$ samples are due to disorder-induced Raman scattering (Ref. 24). In (b) and (c) the polarization dependence is shown. We subtract a Lorentzian fit to the phonon peak in order to isolate these structures and to study the polarization dependence for a $\langle 100 \rangle$ surface. The relative intensity scales of (b) and (c) are the same. Details are given in the text.

In terms of the CPA this is completely analogous to the problem of classical conduction through mixtures, known as effective medium theory, introduced by Bruggeman.[50] The effective medium theory is equivalent to the CPA presented here and has been extensively discussed.[51–55] The effective medium model for a binary system has a percolation threshold of 1/3, regardless of the real topology of the lattice. The concept of percolation for an isotopically disordered lattice has, in some cases, physical consequences for the dynamics of the modes and has already been studied for simple lattices in two and three dimensions by means of direct diagonalization of large random matrices,[56] with emphasis on the behavior of acoustic phonons. We performed calculations based on Eq. (3) for a two-isotope crystal as a function of the concentration and found that the CPA convergence becomes poor at the percolation threshold in the region of the optical phonon branches,[57] as expected. We are currently studying samples with the appropiate mass content to study experimentally this effect, as well as performing calculations to clarify (i) the lattice dynamics in the percolation region where the CPA is expected to fail, (ii) possible effects on optical phonons observable with Raman spectroscopy, and (iii) the selection rules involved in the disorder-induced Raman scattering shown in Fig. 12.[57]

Last but not least, we mention that the related problem of the dependence of electronic gaps of Ge on isotopic mass still presents some complications. These phenomena are complementary of those discussed so far. The electronic bands are renormalized through the first order (*e*-ph) Hamiltonian in second-order (self-energy term) and also the second-order electron–two-phonon interaction taken in first order (Debye-Waller terms).[18,41–44] The disorder-induced self-energy of the phonons is expected to have negligible effect on the mass dependence of the gaps: The shifts are governed by the average mass. This produces the $E \sim 1/\sqrt{\overline{m}}$ behavior reported for bound excitons in Refs. 18, 22, and 23. However, the mass dependence of the $E_1$ (Ref. 34) gap at low temperatures (determined by spectroscopic ellipsometry[45]) is larger than that predicted in the one-electron calculation.[18] In Ref. 18 this was attributed to the poor quality of the then available $^{70}$Ge sample. However, we have obtained new experimental data with improved statistics as well as sample quality. In Fig. 13 we show the energy of the $E_1$ gap of Ge obtained at $T = 10$ K vs mass for the five available samples. The results, which agree with the less accurate ones reported in Ref. 18; are still larger that the theoretical expectations. Excitonic effects[46] may have to be included in the calculations to obtain the correct shift with isotopic mass. More details will be published elsewhere.[58]

Further interesting effects of isotopic substitution should result from investigations of low dimensional structures. The possibility of growing isotopic superlattices, quantum wires, or quantum dots has been proposed and analyzed recently.[60] Band folding effects have been predicted for phonons in isotopic superlattices[61] and localization phenomena should appear (based on the reduced dimensionality) in single plane structures, quantum wires and dots.[60] Those features, when observed, should provide textbooklike examples of localization in lattice dynamics and yield additional information on force constants and bond polarizabilities.

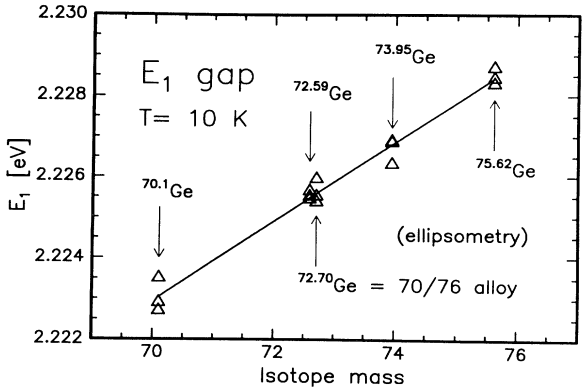


FIG. 13. The $E_1$ electronic gap of Ge at $T = 10$ K obtained for several values of $\overline{m}$ from conventional fitting procedures of ellipsometric data (Ref. 59). The mass dependence of the gap is somewhat larger than that expected from the one-electron plus (*e*-ph) interaction picture (Ref. 43). The different experimental points at each mass represent different measurements with different alignments so as to check for reproducibility (Ref. 45).

*Note added in proof.* In Ref. 24 only the incoherent part of the disorder-induced scattering was calculated. There is also a coherent part which is obtained from the spectral function of the $\mathbf{k} = \mathbf{0}$ phonons and was not included in Ref. 24. We have recently found that inclusion of this component improves the agreement between theory and the data of Fig. 12.

## ACKNOWLEDGMENTS

We wish to thank H. Hirt, M. Siemers, and P. Wurster for technical assistance as well as X. Breitschwerdt and X. König for expert help with the IR-Fourier-transform interferometer. Special thanks are given to Martyn Chamberlain for a critical reading of the manuscript and to Professor V. I. Ozhogin for providing isotopically enriched Ge. We are also thankful to H. V. Klapdor-Kleingrothaus, S. T. Belyaev, and V. Lebedev for the $^{76}$Ge crystal. This work was partially supported by U.S. NSF Grant No. DMR91-15856.

[1] V. F. Agekyan, V. M. Asnin, A. M. Kryukov, I. I. Markov, N. A. Rud', V. I. Stepanov, and A. B. Churilov, Fiz. Tverd. Tela (Leningrad) **31**, 101 (1989) [Sov. Phys. Solid State **31**, 2082 (1989)].

[2] C. H. Grein and M. Cardona, Phys. Rev. B **45**, 8328 (1992).

[3] F. Yonezawa, in *The Structure and Properties of Matter*, edited by T. Matsubara, Springer Series in Solid State Sciences Vol. 28 (Springer, Berlin, 1982), p. 383.

[4]E. N. Economou, in *Green's Functions in Quantum Physics*, Springer Series in Solid State Sciences Vol. 7, edited by M. Cardona, P. Fulde, and H. J. Queisser (Springer, Heidelberg, 1979).
[5]T. H. Geballe and G. W. Hull, Phys. Rev. **110**, 773 (1958).
[6]G. A. Slack, Phys. Rev. **105**, 832 (1957).
[7]P. G. Klemens, Proc. Phys. Soc. London A **68**, 1113 (1955).
[8]A. T. Collins, S. C. Lawson, G. Davies, and H. Kanda, Phys. Rev. Lett. **65**, 891 (1990).
[9]R. Berman, Phys. Rev. B **45**, 5726 (1992).
[10]T. R. Anthony, W. F. Banholzer, J. F. Fleischer, Lanhua Wei, P. K. Kuo, R. L. Thomas, and R. W. Pryor, Phys. Rev. B **42**, 1104 (1990).
[11]K. C. Hass, M. A. Tamor, T. R. Anthony, and W. F. Banholzer, Phys. Rev. B **45**, 7171 (1992).
[12]K. C. Hass, M. A. Tamor, T. R. Anthony, and W. F. Banholzer, Phys. Rev. B **44**, 12046 (1991).
[13]H. D. Fuchs, C. H. Grein, C. Thomsen, and M. Cardona, Phys. Rev. B. **43**, 4835 (1991).
[14]H. D. Fuchs, C. H. Grein, R. I. Devlen, J. Kuhl, and M. Cardona, Phys. Rev. B **44**, 8633 (1991).
[15]W. Weber, Phys. Rev. Lett. **33**, 371 (1974).
[16]W. Weber, Phys. Rev. B **15**, 4789 (1977).
[17]G. Nilsson and G. Nelin, Phys. Rev. B **3**, 364 (1971).
[18]S. Zollner, M. Cardona, and S. Gopalan, Phys. Rev. B **45**, 3376 (1992).
[19]M. Cardona, C. H. Grein, H. D. Fuchs, and S. Zollner, J. Non-Cryst. Solids **141**, 257 (1992).
[20]H. D. Fuchs, C. H. Grein, M. Cardona, W. L. Hansen, K. Itoh, and E. E. Haller, Solid State Commun. **82**, 225 (1992).
[21]H. D. Fuchs, C. H. Grein, M. Bauer, and M. Cardona, Phys. Rev. B **45**, 4065 (1992).
[22]G. Davies, E. C. Lightowlers, K. Itoh, W. L. Hansen, E. E Haller, and E. E. Ozhogin, Semicond. Sci. Technol. **7**, 1271 (1992).
[23]P. Etchegoin, J. Weber, M. Cardona, W. L. Hansen, K. Itoh, and E. E. Haller, Solid State Commun. **83**, 843 (1992).
[24]H. D. Fuchs, P. Etchegoin, M. Cardona, K. Itoh, and E. E. Haller, Phys. Rev. Lett. **70**, 1715 (1993).
[25]G. Davies, J. Hartung, V. Ozhogin, K. Itoh, W. L. Hansen, and E. E. Haller, Semicond. Sci. Technol. **8**, 127 (1993).
[26]I. M. Lifshitz, Nuovo Cimento **3**, Suppl., 716 (1956).
[27]P. G. Dawber and R. J. Elliott, Proc. R. Soc. London A **273**, 222 (1963).
[28]P. G. Dawber and R. J. Elliott, Proc. Phys. Soc. London **81**, 453 (1963).
[29]R. J. Elliott and P. Pfeuty, J. Phys. Chem. Solids **28**, 1789 (1967).
[30]R. J. Elliott, J. A. Krumhansl, and P. L. Leath, Rev. Mod. Phys. **46**, 465 (1974).
[31]S. Gironcoli and S. Baroni, Phys. Rev. Lett. **69**, 1959 (1992).
[32]K. Itoh, W. L. Hansen, E. E. Haller, J. W. Farmer, V. I. Ozhogin, A. Rudnev, and A. Tikhomirov, J. Mater. Res. **8**, 1341 (1993).
[33]D. E. Aspnes and A. A. Studna, Appl. Phys. Lett. **39** (4), 316 (1981).
[34]D. E. Aspnes and A. A. Studna, Phys. Rev. B **27**, 985 (1983).
[35]A. Isihara, in *Electron Liquids*, edited by M. Cardona, Springer Series in Solid State Science Vol. 96 (Springer-Verlag, London, 1993), p. 73, and references therein.
[36]J. C. Hensel, T. G. Phillips, G. A. Thomas, and T. M. Rice, in *Solid State Physics*, edited by H. Ehrenreich, F. Seitz, and D. Turnbull (Academic, New York, 1977), Vol. 32.
[37]*Electron – Hole Droplets in Semiconductors*, Modern Problems in Condensed Matter Series Vol. 6, edited by C. D. Jeffries and L. V. Keldysh (North-Holland, Amsterdam, 1983).
[38]M. Cardona, in *Light Scattering in Solids* II, Topics in applied Physics Vol. 50, edited by M. Cardona and G. Güntherodt (Springer-Verlag, Berlin, 1982), p. 19.
[39]Recent supercell calculations performed by us (by means of the *equation of the motion* method) suggest that the energy shift of $TO_L$ is positive. We are presently checking this result.
[40]The exact shape of the experimental curve depends of course on the chosen laser energy. Intermediate state resonances may enhance certain regions of the spectrum.
[41]M. Cardona and S. Gopalan, in *Progress on Electron Properties of Solids*, edited by R. Girlanda (Kluwer, Dewenter, The Netherlands, 1989), p. 51, and references therein.
[42]P. Lautenschlager, P. B. Allen, and M. Cardona, Phys. Rev. B **31**, 2163 (1985).
[43]S. Gopalan, P. Lautenschlager, and M. Cardona, Phys. Rev. B **35**, 5577 (1987).
[44]M. L. Cohen and D. J. Chadi, in *Handbook of Semiconductors*, edited by M. Balkanski (North-Holland, Amsterdam, 1980), Vol. 2, p. 155.
[45]D. E. Aspnes and A. A. Studna, Rev. Sci. Instrum. **49**, 292 (1978).
[46]M. L. Cohen and J. R. Chelikowsky, in *Electronic Structure and Optical Properties of Semiconductors*, edited by M. Cardona, Springer Series in Solid-State Science Vol. 75 (Springer-Verlag, Berlin, 1988).
[47]B. I. Shklovskii and A. L. Efros, *Electronic Properties of Doped Semiconductors*, Springer Series in Solid-State Science Vol. 45 (Springer, New York, 1984).
[48]M. B. Isichenko, Rev. Mod. Phys. **64**, 961 (1992).
[49]R. M. Martin and F. L. Galeener, Phys. Rev. B **23**, 3071 (1981).
[50]D. A. G. Bruggeman, Ann. Phys. (Leipz.) **24**, 636 (1935).
[51]R. Landauer, J. Appl. Phys. **23**, 779 (1952).
[52]W. F. Brown, Handb. Phys. **17**, 104 (1956).
[53]E. H. Kerner, Proc. Phys. Soc. London B **69**, 802 (1956).
[54]J. A. Krumhansl, in *Amorphous Magnetism*, edited by H. O. Hooper and A. M. De Graff (Plenum, New York, 1973), p. 15.
[55]S. Kirkpatrick, Rev. Mod. Phys. **45**, 574 (1973).
[56]J. Canisius and J. L. van Hemmen, J. Phys. C **18**, 4873 (1985).
[57]P. Etchegoin, E. Artacho, and M. Cardona (unpublished).
[58]P. Etchegoin, H. D. Fuchs, M. Cardona, K. Itoh, and E. E. Haller (unpublished).
[59]L. Viña, S. Logothetidis, and M. Cardona, Phys. Rev. B **15**, 2127 (1977).
[60]M. Cardona, P. Etchegoin, H. D. Fuchs, and P. Molinàs-Mata, J. Phys. Condens. Matter **5**, A61 (1993).
[61]H. D. Fuchs, P. Molinas-Mata, and M. Cardona, Superlatt. Microstruc. (to be published).